applied sciences

MDPI

Article

Sequential Low-Light Image Enhancement Using Eigenvalue-Based Gamma Correction and Laplacian Feature Map-Based Transmission Map

Hosang Lee

Department of Computer Engineering, Kyungnam University, Changwon-si 51767, Gyungsangnam-do, Republic of Korea; hslee7092@kyungnam.ac.kr

Abstract

Low-light images are typically captured under adverse conditions, such as nighttime environments or low-contrast settings, which severely hinder visual understanding and object recognition. Although various deep learning and image signal processing techniques have been proposed to address this issue, low-light image enhancement remains a challenging task due to the lack of ground-truth reference images and the diverse range of real-world degradation phenomena. To overcome these limitations, this paper proposes a novel low-light image enhancement framework utilizing an eigenvalue-based gamma correction method based on the ratio of the 1st and 2nd eigenvalues, which effectively captures the inherent characteristics of the input image. Furthermore, because image enhancement processes inevitably amplify background noise, this paper incorporates a specialized denoising method inspired by dehazing theory to mitigate this side effect. A critical challenge in mathematical dehazing models is the accurate estimation of the transmission map, which is often distorted by strong light components in low-light scenes, leading to undesirable halo effects and color distortion. To solve this, this paper introduces a Laplacian feature map-based transmission map, leveraging the fact that Laplacian edge components remain independent of ambient illumination. Extensive experimental evaluations demonstrate that the proposed method outperforms state-of-the-art approaches, delivering superior visual quality in both objective and subjective assessments.

Keywords: low-light image enhancement; eigenvalue; gamma correction; Laplacian feature map; denoising; dehazing

1. Introduction

Images inherently reflect the conditions under which they are captured. When the environment is excessively dark, the resulting images are consequently dim and poorly illuminated. Enhancing low-light images often amplifies background noise, making it exceptionally difficult to achieve clear visual results. While numerous studies have focused on improving low-light image contrast using machine learning and traditional image processing techniques, training neural networks remains challenging due to the absence of ground-truth reference images and the wide diversity of real-world low-light environments. Nevertheless, accurate object recognition in low-light conditions is critical for computer vision and image recognition systems. To enhance image contrast, conventional techniques such as histogram equalization and gamma correction have been widely utilized. Huang et al. [1] proposed a low-light image enhancement method using adaptive gamma correction and cumulative intensity distribution. Their approach enhances

Check for updates

Academic Editor: Pedro Couto

Received: 25 September 2026
Revised: 20 October 2026
Accepted: 20 October 2026
Published: 22 October 2026

Copyright: © 2026 by the author. Licensee MDPI, Basel, Switzerland. This article is an open access article distributed under the terms and conditions of the Creative Commons Attribution (CC BY) license.

low-light images by employing a modified histogram method based on gamma correction and the probability distribution of luminance. Although this method effectively enhances moderately low-light images, its performance degrades significantly when processing extremely dark regions, such as nighttime scenes, resulting in low-quality outputs. Ma et al. [2] proposed a low-light image enhancement algorithm based on the HSV color model. To improve the contrast of low-light images, they utilized the saturation and intensity components, which are trained through deep neural networks [2]. Although this method enhances low-light images, the resulting images often retain a dim effect, and heavily dark regions remain underexposed. Dong et al. [3] proposed a low-light image improvement method via a dehazing algorithm. Although this method excels in processing speed, some enhanced images suffer from ringing artifacts and distorted areas. Tang et al. [4] suggested a low-contrast image enhancement method using Retinex theory with a guided filter. In this work, to reduce the halo effect in enhanced low-light images, they employed an improved Retinex-based enhancement algorithm utilizing a guided filter in the HIS color space [4]. Fu et al. [5] proposed a low-light image enhancement method using a probabilistic approach with simultaneous illumination and reflectance estimation. This approach properly enhances low-light images in the linear domain by simultaneously estimating illumination and reflectance, such as through maximum a posteriori estimation [5]. However, images enhanced by this method still suffer from color distortion. Yang et al. [6] suggested a low-light image enhancement method using a semi-supervised approach, specifically a deep recursive band network. Jobson et al. [7] proposed an image enhancement method utilizing multiscale Retinex. Although this method enhances low-light images, some outputs suffer from ringing artifacts. Kimmel et al. [8] suggested an image enhancement method using a variational framework for Retinex. Although this method sufficiently enhances low-light images, it introduces distorted regions, such as oversaturation. Zhou et al. [9] enhanced low-light images using generative perceptual priors (GPP-LLIE). While effective, its enhancement capability is limited in extremely dark regions. Liu et al. [10] introduced a Retinex-based algorithm combining unrolling and adjustment. Although this method is generally suitable, the enhancement effect remains insufficient for severely dark low-light images. Wei et al. [11] proposed ClassLIE, a low-light image enhancement method combining the potential of convolutional neural networks and transformers. While this method performs properly, enhanced images often exhibit color distortion in sky regions [11]. Jiang et al. [12] suggested a diffusion-model-based low-light image enhancement method, which achieves remarkable performance. Yin et al. [13] proposed a degraded low-light image enhancement method using a structure-guided diffusion transformer, utilizing wavelet sub-bands for denoising. Finally, Li et al. [14] introduced the spatially adaptive illumination-guided transformer (SAIGFormer) with dynamic integral image representation for low-light enhancement, demonstrating exceptional performance. Zeng et al. [15] proposed a low-light image enhancement method using physics-guided rectified flow. Although this method can enhance low-light images, its enhancement effect is relatively limited. Han et al. [16] proposed a low-light image enhancement method through controllable low-light enhancement (CLE), demonstrating remarkable performance even for extremely dark images. Huang et al. [17] suggested a low-light image enhancement method using latent diffusion models. Although the resulting images are brighter, they still appear somewhat dark and dim. Chen et al. [18] enhanced low-light images by combining diffusion models and Retinex theory. While this method successfully brightens the image, it introduces color distortion in the enhanced output. Wu et al. [19] utilized joint Retinex and semantic priors within a diffusion model for low-light image enhancement. Although this method performs well overall, minor color distortion areas appear in certain images. Zou et al. [20] proposed a low-light image enhancement method using a wavelet state-space

model, achieving exceptional performance. Moreover, Wu et al. [21] enhanced low-light images using light-aware contrastive learning by leveraging negative information and accounting for uneven illumination. While this method exhibits excellent performance, some images still contain over-saturated regions. Li et al. [22] enhanced low-light images using a global-to-local Mamba architecture for feature extraction. Although this method effectively enhances low-light images, the resulting outputs occasionally contain color-distorted regions. Cai et al. [23] proposed a one-stage Retinex-based transformer for low-light enhancement. While this method performs well overall, some enhanced images suffer from over-saturated regions. Yin et al. [24] enhanced low-light images by combining an iterative learning mechanism with Retinex theory. Although this method performs adequately, it exhibits degradation in extremely dark or exposed areas [24]. Lan et al. [25] introduced an efficient diffusion-based low-light enhancer. While capable of proper enhancement, certain images contain noticeable artifacts [25]. Zeng et al. [26] utilized a diffusion model with semantic priors for low-light enhancement. Although effective, relying on semantic and edge maps generated by the Segment Anything Model (SAM) imposes limitations regarding structural diversity [26]. Ma et al. [27] proposed a self-calibrated illumination learning framework, which enhances low-light images quite naturally. Hou et al. [28] introduced a global-structure-aware diffusion procedure that enhances low-light images suitably. Finally, Weng et al. [29] proposed an implicit Retinex-aware method utilizing global and local state spaces, featuring a local enhanced state space module (LESSM) and an implicit Retinex-aware selective kernel module (IRSK). Although this method yields favorable enhancement results, it shares limitations related to prior dependency [29]. Ding et al. proposed low-light remote sensing image enhancement using a priors-guided latent residual diffusion model [30]. This method enhances low-light images suitably; however, in some images, there are oversaturated regions. He et al. proposed a low-light image enhancement method using depth residuals and transformer techniques [31]. This method enhances low-light images properly. Sun et al. enhanced low-light images using event-based illumination estimation [32]. Although this method enhances low-light images suitably, in the case of severely dark images, the enhancing effect is somewhat low. Wu et al. suggested a low-light image enhancement method using a semantic-aware knowledge-guided framework (SKF) [33]. This method enhances low-light images properly. Wang et al. enhanced low-light images using generalized enhancement for understanding (GEFU) the low-light image [34]. The enhanced images produced by this method have good quality. Wang et al. suggested a low-light image enhancement method using illumination-aware gamma correction and a complete image-modelling network [35]. Although this method is able to enhance low-light images suitably, there are limitations such as color distortion [35]. Wu et al. [36] proposed a low-light image enhancement method using a Retinex-based deep unfolding network (URetinex-Net). Although this method effectively enhances low-light images, some outputs occasionally contain color-distorted regions [36]. Xu et al. [37] proposed a signal-to-noise-ratio-aware method for low-light enhancement, yielding images of remarkable quality. Yan et al. [38] enhanced low-light images using horizontal, vertical, and intensity spaces. While this method performs properly, extremely dark images still retain a hazy or dim effect even after enhancement. Yi et al. [39] introduced a generative-diffusion-model-based low-light enhancement method, achieving suitable performance. Guo et al. [40] enhanced low-light images using the maximum value of each color channel; although efficient, this method tends to produce over-saturated regions in the enhanced outputs [40]. Ying et al. [41] proposed a bio-inspired multi-exposure fusion framework, which properly enhances low-light images while occasionally suffering from over-saturation in certain areas [41]. Moreover, Ren et al. [42] utilized a camera response model for low-light image enhancement, achieving appropriate and reliable en-

hancement results. Li et al. [43] properly enhanced low-light images using a convolutional neural network, achieving notable enhancement performance. Wang et al. [44] proposed a naturalness-preserved enhancement method designed for non-uniform illumination images, demonstrating favorable performance. Ma et al. [45] introduced a self-calibration-based low-light enhancement method; while it delivers promising results, some enhanced images still exhibit over-saturated regions. Jiang et al. [46] proposed a semantic-aware low-light image enhancement method based on the color space, producing visually pleasing results of high quality. To date, numerous studies have attempted to address low-light image enhancement using machine learning and traditional image processing techniques. However, machine learning-based approaches face inherent limitations, particularly regarding training datasets, as constructing comprehensive low-light datasets is a complex and challenging task. Furthermore, even when sufficient training data is secured, fully capturing the diverse and unpredictable conditions of real-world low-light environments remains exceedingly difficult. In addition, because the enhancement process inevitably amplifies background noise, a dedicated denoising procedure is consistently required.

Therefore, this paper proposes a novel low-light image enhancement method utilizing eigenvalue-based gamma correction for contrast stretching and a Laplacian feature map for dehazing-based denoising.

2. Proposed Method

Due to poor illumination, low-light images typically suffer from dimness and noise. Consequently, when such images are enhanced, the amplified noise from the original input often results in an unclear, hazy appearance. To address this limitation, this paper proposes a novel low-light image enhancement framework consisting of two main procedures: a color channel compensation procedure utilizing eigenvalue-based gamma correction and a noise reduction procedure employing a Laplacian feature map for the transmission map.

2.1. Contrast Enhancement

Low-light images typically appear dark and noisy. Consequently, even after enhancement, the resulting outputs often exhibit a hazy appearance due to amplified noise particles. Therefore, effectively enhancing low-light images requires an adaptive parameter that accurately reflects the inherent characteristics of the image. Lee [47] successfully improved degraded sandstorm images using image eigenvalues. The eigenvalue of an image can properly capture its underlying characteristics. Specifically, if an image is extremely dark, its first eigenvalue yields a low value, whereas bright or naturally illuminated images yield a high value. Motivated by this phenomenon, this paper proposes a low-light image enhancement method utilizing the image's eigenvalues. The eigenvalue of the image is obtained as follows:

$$\xi^c = |eig(I^c)|, \tag{1}$$

where $|\cdot|$ denotes the absolute value operator, and ξ^c represents the eigenvalue of each color channel obtained through the eigenvalue extraction function, $eig(\cdot)$, applied to the color image. To compute the eigenvalues for each color channel, this paper first resizes the input image based on its smaller spatial dimension to maintain computational efficiency. Subsequently, this paper constructs the intensity distribution matrix for each channel. The eigenvalues of the color channels are then extracted to represent the local intensity distribution and dynamic exposure characteristics, which serve as the foundation for adaptive gamma correction. Specifically, to extract the eigenvalues for each color channel, the image dimensions are adjusted according to the smaller size between its width and height. After extracting the eigenvalues per channel, this paper takes the absolute value to eliminate any imaginary parts and uses them as weighting factors. Finally, the ratio between

the first and second eigenvalues is computed and applied as a weighting factor for image stretching, where the image size remains identical to the original resolution. I^c is the input, with $c \in \{r, g, b\}$. Using Equation (1), the absolute eigenvalues can be successfully obtained. Although an image's eigenvalues can be directly utilized for low-light enhancement, they often span a wide range of values. To ensure stable application, this paper proposes using the ratio between the first and second eigenvalues. The first eigenvalue component primarily captures the background characteristics of the image, while the second eigenvalue reflects additional inherent features. Figure 1 illustrates the relationship between image contrast and its first and second eigenvalues according to varying brightness levels. As demonstrated in Figure 1, brighter images yield higher eigenvalues, whereas darker images result in lower eigenvalues. Motivated by this relationship, this paper introduces an enhancement ratio derived from the two eigenvalues. This ratio is formulated as follows:

$$r^c = \frac{\xi_1^c}{\xi_2^c}, \tag{2}$$

where ξ_1^c and ξ_2^c denote the first and second eigenvalues of the image, and r^c represents the ratio between the two eigenvalues. Furthermore, since extracting eigenvalues from extremely dark images is challenging, an inverted image is utilized to address this issue. By applying Equation (2) alongside the gamma correction technique, low-light images can be effectively enhanced. However, for extremely dark images, the ratio values may fluctuate across a wide range. To address this instability, this work proposes a stable enhancement method utilizing a logarithmic function. Due to the properties of the logarithmic function, large values are compressed into a stable and manageable range. Therefore, to stably incorporate the eigenvalue information, the modified ratio is formulated as follows:

$$r_m^c = \log_2(1 + r^c), \tag{3}$$

$$I_s^c(x) = \{I^c(x)\}^{\frac{1}{r_m^c}}, \tag{4}$$

where r_m^c denotes the modified ratio for each color channel, r^c represents the initial eigenvalue ratio, with $c \in \{r, g, b\}$, and I_s^c represents the stretched image obtained via gamma correction using this ratio. By applying Equation (3), low-light images can be stably enhanced. Moreover, assuming that the pixel intensity range of the image is normalized to [0, 1], applying $\log_2$ enables natural image enhancement. However, extremely dark images (approaching pure black) may yield an eigenvalue of zero during extraction, leading to computational errors. Specifically, for extremely dark or non-color (grayscale) images, the pixel intensity variations across regions become negligible, causing the corresponding eigenvalues to degenerate toward zero. As illustrated in Figure 2, which compares the eigenvalues of an extremely dark image and its reversed counterpart, the eigenvalue of the dark image remains near zero, whereas that of the reversed version does not. Therefore, to resolve this issue, this work proposes a robust eigenvalue calculation method utilizing the inverted image and the maximum intensity value. To robustly handle severely under-exposed scenes, we introduce an image inversion step prior to eigenvalue analysis. Specifically, the inverted image is obtained by subtracting the pixel values of the resized input image from the maximum intensity level. The primary role of this inversion is to overcome the limitation where extremely dark regions yield near-zero eigenvalues, which otherwise obstruct reliable feature extraction. To address severely under-exposed or nearly black regions without causing structural collapse or color distortion, the proposed method incorporates an adaptive inversion strategy. First, regarding the concern that image inversion could yield an artificial uniform white field for completely black images, this paper

emphasizes that the inverted image is not directly rendered as the final output; rather, it is exclusively utilized to extract eigenvalues that serve as weighting factors for the original, pre-inversion image. Second, the maximum and second-largest eigenvalues are computed and processed independently on a per-channel basis, thereby ensuring precise color balance and reproduction. Third, image inversion is applied conditionally—triggered only when the largest or second-largest eigenvalue per channel approaches zero—which reliably preserves the authentic color and tonal characteristics of the original input. Finally, to mitigate potential blown highlights and detail loss, the framework applies the final gamma correction, effectively stabilizing the dynamic range and minimizing information loss. Transforming the dark image into its inverted domain effectively highlights the hidden structural and illumination details, enabling the proposed eigenvalue-based gamma correction and Laplacian transmission estimation to operate with high stability and precision. As illustrated in Figure 3, applying Equations (1)–(3) allows low-light images to be enhanced naturally through gamma correction. In Figure 3, the first column displays the original low-light images, while the second column shows the enhanced outputs. Furthermore, the incorporation of a refinement procedure effectively reduces and compensates for oversaturated regions, preventing color distortion. Nevertheless, because the enhancement process inevitably amplifies noise particles, the resulting images may still exhibit a hazy appearance, as observed in the second row of Figure 3. To address this limitation, an additional noise reduction component is necessary.

(a)



		Red	Green	Blue
Eigenvalue	1st	51.539	43.681	37.153
	2nd	8.931	8.570	10.981

(b)



		Red	Green	Blue
Eigenvalue	1st	145.953	129.106	97.394
	2nd	13.817	13.543	17.366

Figure 1. The relationship between image brightness and eigenvalues: (**a**) Low-light image and its 1st and 2nd eigenvalues; (**b**) bright image and its 1st and 2nd eigenvalues.

(a)



		Red	Green	Blue
Eigenvalue	1st	0	0	0
	2nd	0	0	0

(b)



		Red	Green	Blue
Eigenvalue	1st	302.518	302.518	302.518
	2nd	11.110	11.110	11.110

(c)



Eigenvalue	1st	0
	2nd	0

Figure 2. Conditions under which the 1st eigenvalue of the image becomes zero: (**a**) the 1st and 2nd eigenvalues of a grayscale image; (**b**) the 1st and 2nd eigenvalues of an inverted image; (**c**) the 1st and 2nd eigenvalues of an all-black image.



Figure 3. Comparison of low-light images by procedure. Top row: original low-light image; bottom row: improved low-light image using Equations (3) and (4) with gamma correction.

2.2. Noise Reduction Using Laplacian Feature Map-Based Transmission Map

Enhanced low-light images often appear hazy due to amplified background noise. When an image is brightened, noise particles are simultaneously magnified, resulting in degraded visual quality. Therefore, achieving natural and effective enhancement requires both a contrast adjustment procedure and a dedicated noise reduction mechanism. To address this haze-like artifact, this paper adopts a dehazing algorithm. While various

image processing techniques and mathematical models—such as conventional gamma correction—have been explored to handle hazy scenes, He et al. [48] proposed a foundational physical scattering model for hazy images. To restore the scene, this method estimates the transmission map, which describes the medium's transmission path of light, and recovers the clear image based on the dark channel prior (DCP) [48]. The transmission map is estimated as follows:

$$t(x) = 1 - \min_{c \in \{r,g,b\}} (\min_{k \in \omega(x)} (\frac{I^c(k)}{A^c})), \tag{5}$$

where t(x) denotes the transmission map, min(·) represents the minimum operator, ω is the local patch (kernel size), I^c represents the color image channel, A^c denotes the atmospheric light as proposed by He et al. [48], and x represents the pixel position. As formulated in Equation (5), He et al. [48] estimated the transmission map based on the dark channel prior. However, when applying this conventional approach to low-light images, extremely bright regions frequently cause severe halo effects and color distortion in the enhanced output. Furthermore, because certain areas of low-light scenes remain difficult to restore completely, a sensitive and robust mechanism is required to achieve natural enhancement. To address these limitations, this paper proposes utilizing a Laplacian feature map for transmission map estimation. Although it is not strictly illumination-invariant, it is well-suited for low-light conditions. Although the Laplacian operator is theoretically sensitive to spatially varying illumination and multiplicative brightness changes—and thus not strictly invariant to non-uniform lighting conditions—it acts as a high-pass filter that effectively suppresses smoothly varying low-frequency components (i.e., global and regional illumination variations) while preserving dominant structural edges.

To mitigate the impact of strong local light sources or uneven illumination, the proposed method incorporates a Laplacian feature map-based transmission map. As demonstrated in Figure 4, proposed experiments under complex low-light scenarios show that the proposed Laplacian-based transmission map maintains strong robustness against non-uniform illumination, ensuring reliable performance even in challenging environments with intense localized light. Although the Laplacian operator inherently extracts high-frequency components—which could potentially amplify noise in low-light conditions—the proposed framework overcomes this limitation through two key steps. First, the resulting Laplacian image undergoes a strict normalization process mapped to the range of [0, 1]. Second, a morphological erosion operation (13 × 13 kernel) is applied to compensate for and smooth out high-frequency fluctuations. This design effectively suppresses noise amplification and ensures that the estimated transmission map remains smooth and robust for subsequent dehazing. Specifically, Laplacian feature maps consist primarily of edge components that are largely robust to illumination variations. The procedure for obtaining the Laplacian-based transmission map is as follows:

$$I^c_{\mathcal{L}f}(x) = N\{\mathcal{L}_f(I^c_s(x))\}, \tag{6}$$

$$\mathrm{I}_d(x) = \min_c\{I^c_{\mathcal{L}f}(x)\}, \tag{7}$$

$$\mathrm{t(x)} = 1 - I_d(x) \tag{8}$$

where $\mathrm{I}^c_{\mathcal{L}f}$ denotes the Laplacian feature map for each color channel, $\mathcal{L}_f(\cdot)$ represents the Laplacian operator with a kernel size of 3 × 3, I_d denotes the dark channel, $\min_c\{\cdot\}$ represents the minimum operation, $\mathrm{N}\{\cdot\}$ denotes the min–max normalization function based on the minimum and maximum values, t(x) represents the transmission map, x is the pixel location, and $\mathrm{c} \in \{\mathrm{r}, \mathrm{g}, \mathrm{b}\}$. Furthermore, since the Laplacian feature map primarily consists

of edge components, this paper applies a morphological erosion operation. Additionally, a Gaussian smoothing filter with a 25 × 25 kernel and a sigma of 6 is employed to refine the transmission map. Figure 5 illustrates the procedure for obtaining the dark channel and transmission map based on the Laplacian feature map. As demonstrated in Figure 5, the transmission map derived from the Laplacian feature map is not invariant to the ambient lighting conditions.

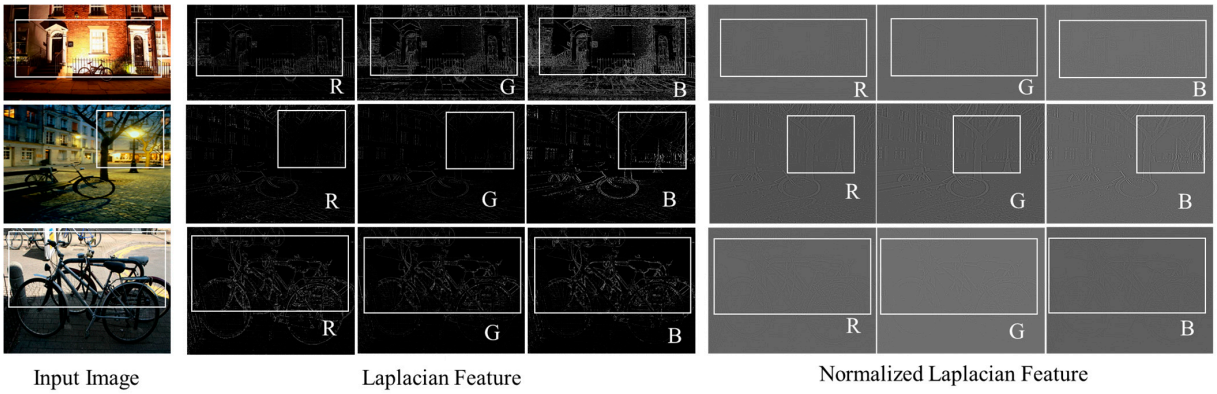


Figure 4. Comparison of Laplacian feature maps under different illumination conditions.

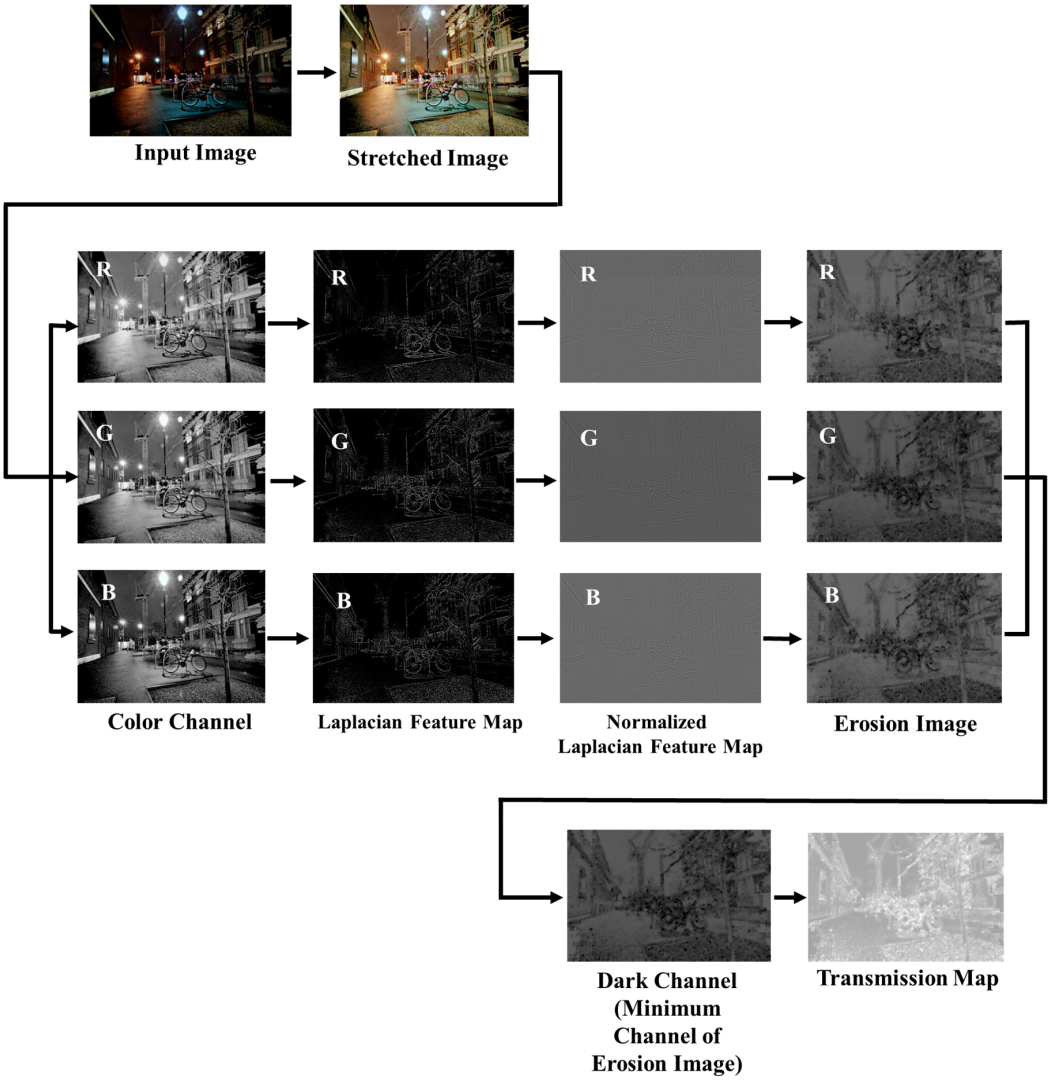


Figure 5. The procedure for obtaining transmission through the Laplacian feature map.

2.3. Image Recovery

Using the stretched image obtained via the proposed eigenvalue-based gamma correction and the Laplacian-feature-based transmission map, the final image is recovered through the atmospheric scattering model [48] as follows:

$$J^c(\mathrm{x}) = \frac{I_s^c(x) - A_s^c(x)}{\max(t(x), 0.1)} + A_s^c(x), \tag{9}$$

where J^c denotes the recovered image, I_s^c means the stretched image, t represents the transmission map, x is the pixel location, $\max(\cdot)$ denotes the maximum operation with a lower bound constant of 0.1 to prevent division by zero, $c \in \{r, g, b\}$, and A_s^c represents the atmospheric light as obtained by the He et al. [48] method of the stretched image. Furthermore, to mitigate the haze-like artifacts, this paper utilizes the normalized stretched image, and unsharp masking using a Gaussian filter is applied to refine the details of the enhanced image in the Value channel of the HSV color space. Equation (9) recovers the low-light image using the color-compensated stretched image, the transmission map, and the atmospheric light estimation introduced by He et al. [48]. Figure 4 illustrates the step-by-step intermediate and final results of the proposed method. As demonstrated in Figure 6, the proposed method exhibits superior performance and robust effectiveness in low-light image enhancement, validating its overall suitability for this task.

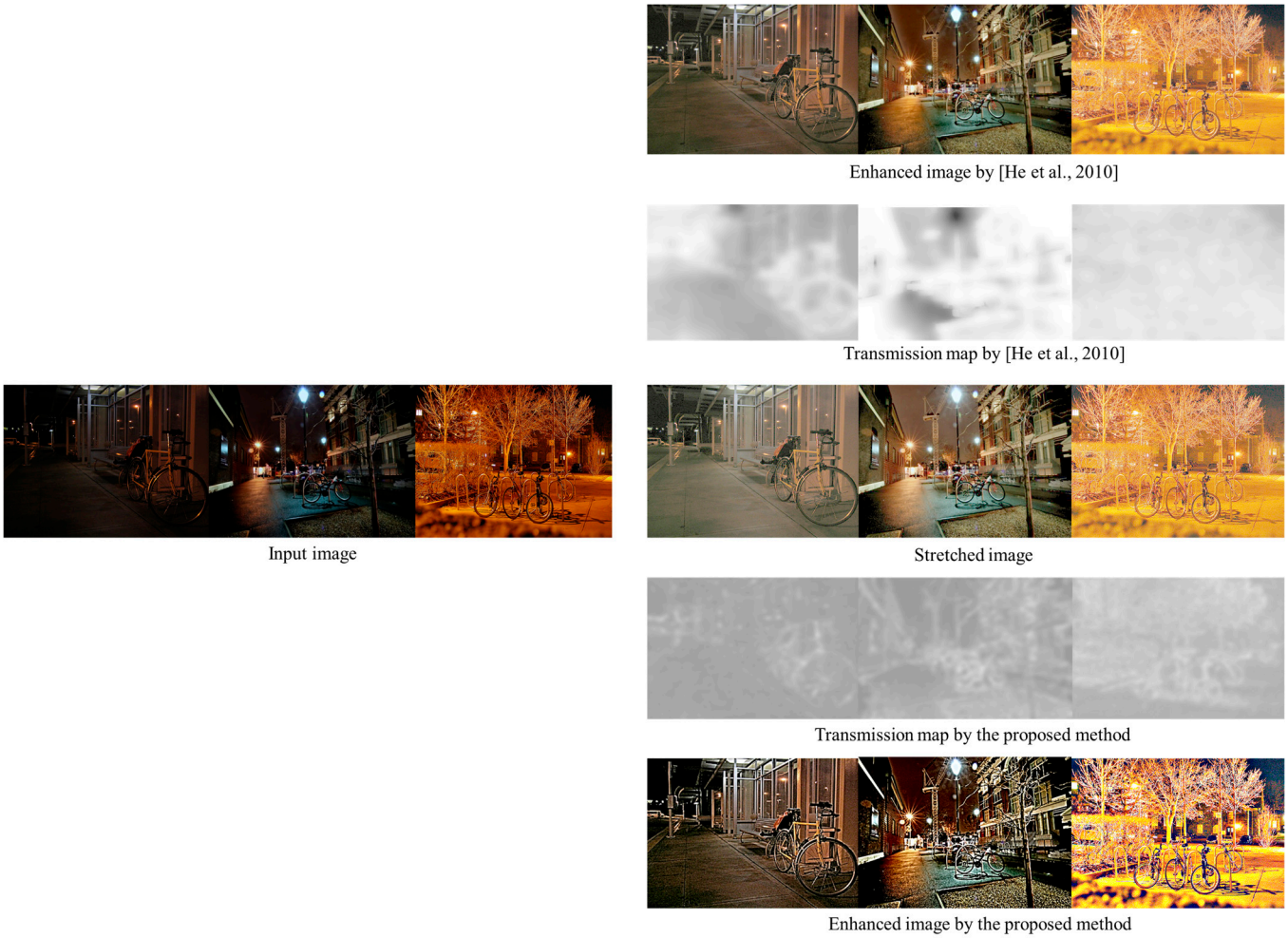


Figure 6. Comparison of each procedure [48].

2.4. Summary

Figure 7 illustrates the overall pipeline of the proposed method. As shown in Figure 7, to naturally enhance low-light images, our method employs an eigenvalue-based gamma correction technique and a Laplacian feature map-based transmission map. Table 1 outlines the overall algorithm of the proposed method. As shown in the table, the proposed approach compensates for the color channels using eigenvalue ratios and utilizes Laplacian feature maps to estimate the transmission map for image enhancement. Furthermore, to evaluate the computational time, Table 2 presents the execution results measured on a system equipped with an Intel® Core™ i7-8700 CPU @ 3.20 GHz, 32 GB RAM, and NVIDIA GeForce GTX 1650, 1660.

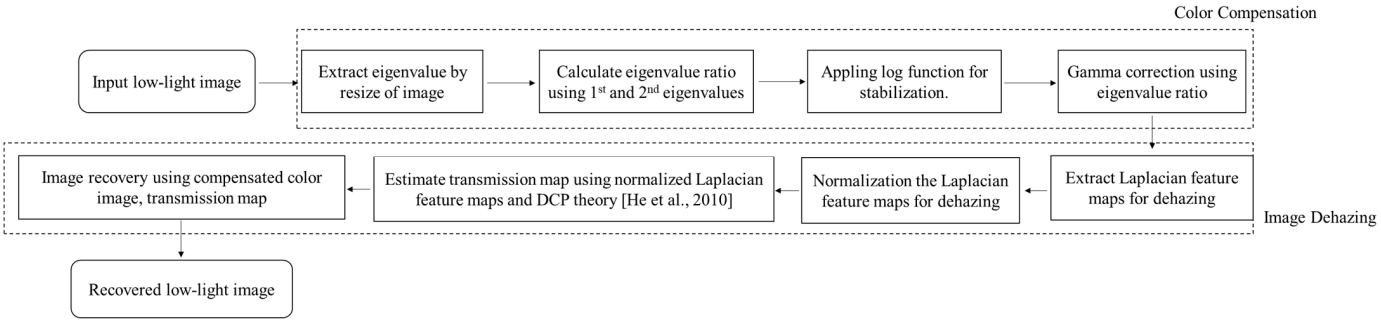


Figure 7. The overall pipeline of the proposed method [48].

Table 1. The overall algorithm of the proposed method.

Input	$I^c(x)$	
		Color Correction
	1	Extract eigenvalue value of each color channel: Equation (1)
	2	Calculate ratio of 1st and 2nd eigenvalues: Equation (2)
	2	Stretching of eigenvalue by log function: Equation (3)
	3	Applying gamma value by reverse gamma value: Equation (4)
		Dehazing
	4	Extract Laplacian feature map: Equation (6)
	5	Normalize Laplacian feature map: Equation (6)
	6	Estimate transmission map using normalized Laplacian feature map and DCP theory [48]: Equations (7) and (8)
	7	Image recovery: Equation (9)
Output	$I^c_{en}(x)$	

Table 2. Calculation time for each method.

Method	Huang et al. [1]	Ying et al. [41]	Dong et al. [3]	Ren et al. [42]	Guo et al. [40]	Li et al. [43]	Jobson et al. [7]
Calculation time(s)	0.046	0.136	0.359	0.139	0.11	2.952	0.334
Method	Wang et al. [44]	Wu et al. [36]	Ma et al. [27]	Haung et al. [17]	Jiang et al. [46]	Lan et al. [25]	PM
Calculation time(s)	8.277	4.543	4.166	109.785	2.648	1.513	1.396

3. Experimental Result

The low-light image is enhanced through a combination of a contrast improvement procedure and a dehazing-based noise reduction procedure. To evaluate the performance of the proposed method, both subjective and objective assessments are conducted. Specifically, this paper utilizes a comprehensive low-light image dataset comprising 12 distinct categories of severely dark images [49]. The dataset consists of 12 categories: 652 dark bicycle, 679 dark boat, 547 dark bottle, 527 dark bus, 638 dark car, 735 dark cat, 648 dark chair, 519 dark cup, 801 dark dog, 503 dark motorbike, 609 dark people, and 505 dark table images, resulting in a total of 7363 severely low-light images without ground truth images [49].

3.1. Subjective Assessment

Low-light images typically suffer from low contrast, appearing dark and dim. To address this issue, various enhancement approaches have been developed. In this section, to comprehensively evaluate the performance of the proposed method, comparative qualitative assessments are conducted against several state-of-the-art techniques based on visual clarity and edge preservation, including those by Dong et al. [3], Ying et al. [41], Wang et al. [44], Jobson et al. [7], Ren et al. [42], Guo et al. [40], Li et al. [43], Huang et al. [1], Wu et al. [36], Huang et al. [17], Lan et al. [25], Jiang et al. [46], and Ma et al. [27], as illustrated in Figures 8–10. As shown in Figures 8–10, the enhanced images produced by Dong et al. [3] often exhibit visual artifacts and show limited enhancement capability for extremely dark scenes. Similarly, the method by Ying et al. [41] suffers from blurring effects and struggles with insufficient luminance restoration in very dark regions. While Wang et al. [44] achieve superior visual quality compared to Dong et al. [3], their approach introduces a noticeable hazy appearance when applied to severely dark inputs. Although Jobson et al. [7] provide reasonable enhancement overall, excessive contrast stretching leads to dim and hazy outputs. Similarly, while Ren et al. [42] perform adequately on moderately dark images, their method results in pronounced haze in extremely dark scenes, as observed in the second row. Guo et al. [40] effectively enhance low-light images, except for extremely dark scenes. Similarly, the method by Li et al. [43] performs adequately, but tends to produce over-exposed (white-out) regions in very dark inputs. The gamma-correction-based method by Huang et al. [1] achieves suitable enhancement overall, though its capability diminishes significantly for extremely dark images. Furthermore, while the method by Wu et al. [36] provides reasonable enhancement, it leaves a dim, hazy appearance when applied to severely dark inputs. Jiang et al. [46], Huang et al. [17], and Lan et al. [25] effectively enhanced low-light images. Ma et al. [27] enhanced low-light images quite well, but these also suffered from a hazy effect in extremely dark regions. In contrast, the enhanced images generated by the proposed method are free from artificial artifacts and over-exposure regions. As demonstrated in Figures 8–10, the proposed method outperforms existing techniques in terms of preventing color distortion and preserving natural brightness.

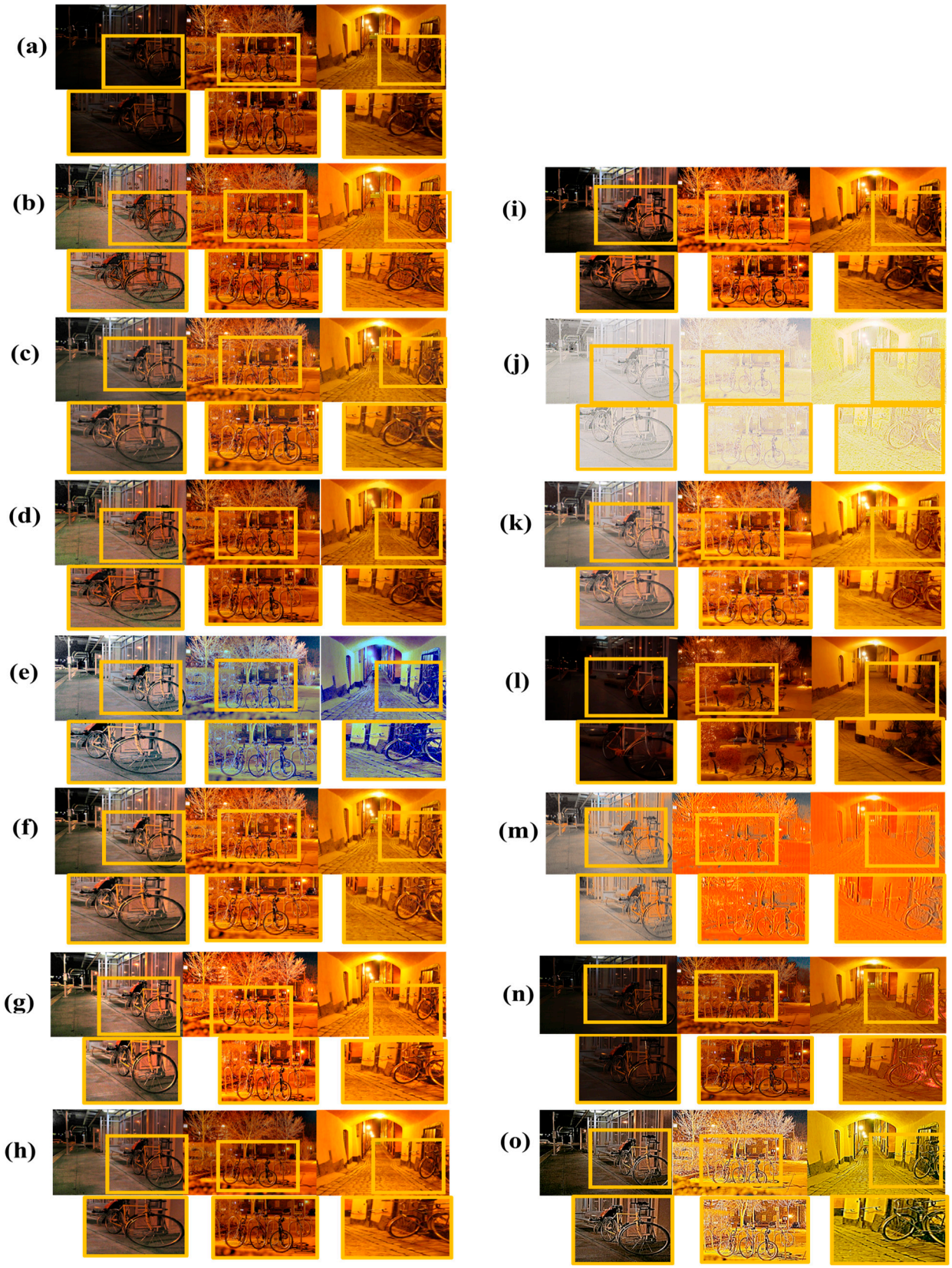


Figure 8. Comparison with state-of-the-art methods and the proposed method: (**a**) input; (**b**) Dong et al. [3]; (**c**) Ying et al. [41]; (**d**) Wang et al. [44]; (**e**) Jobson et al. [7]; (**f**) Ren et al. [42]; (**g**) Guo et al. [40]; (**h**) Li et al. [43]; (**i**) Huang et al. [1]; (**j**) Ma et al. [27]; (**k**) Wu et al. [36]; (**l**) Huang et al. [17]; (**m**) Jiang et al. [46]; (**n**) Lan et al. [25]; (**o**) proposed method.

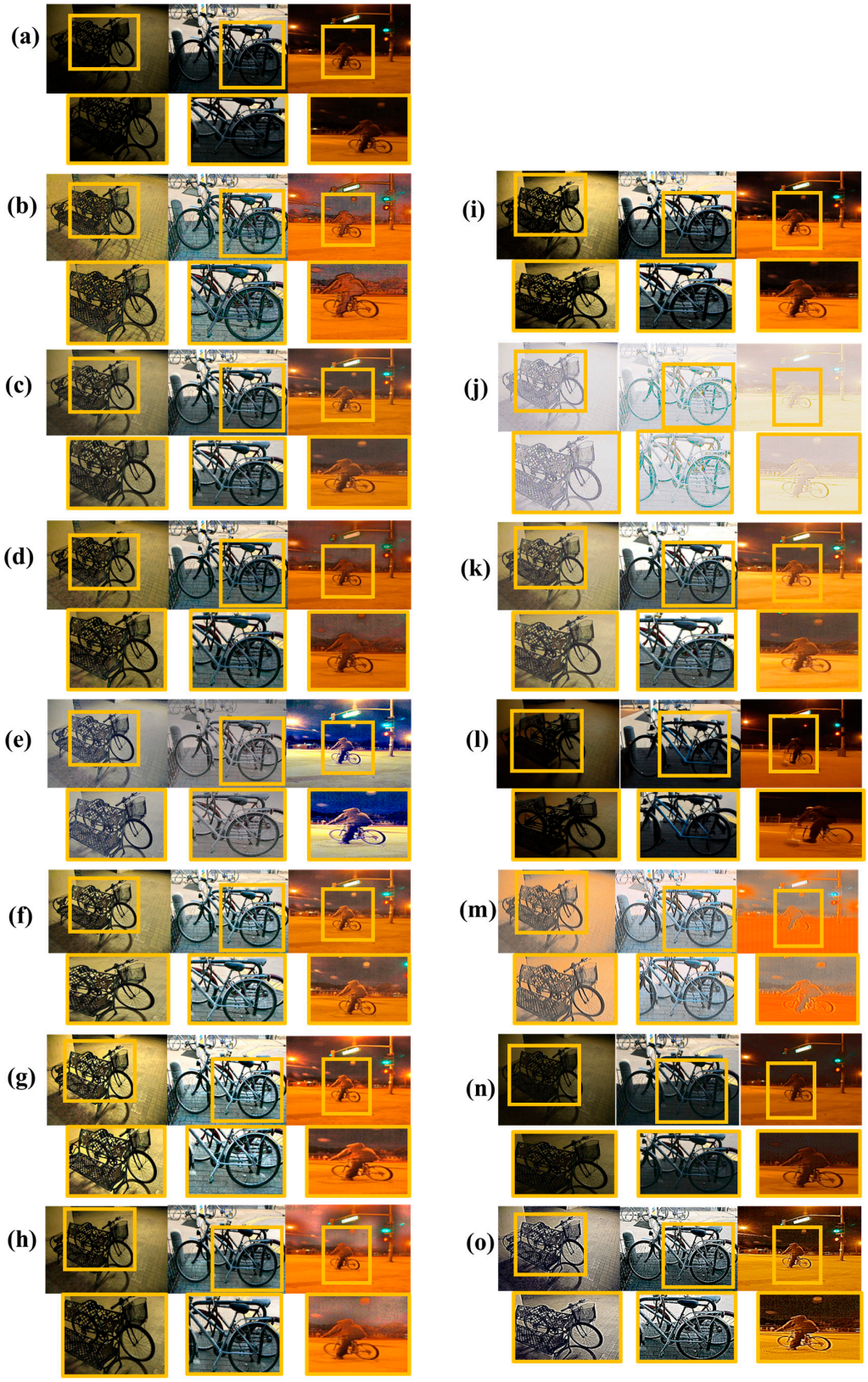


Figure 9. Comparison with state-of-the-art methods and the proposed method: (**a**) input; (**b**) Dong et al. [3]; (**c**) Ying et al. [41]; (**d**) Wang et al. [44]; (**e**) Jobson et al. [7]; (**f**) Ren et al. [42]; (**g**) Guo et al. [40]; (**h**) Li et al. [43]; (**i**) Huang et al. [1]; (**j**) Ma et al. [27]; (**k**) Wu et al. [36]; (**l**) Huang et al. [17]; (**m**) Jiang et al. [46]; (**n**) Lan et al. [25]; (**o**) proposed method.

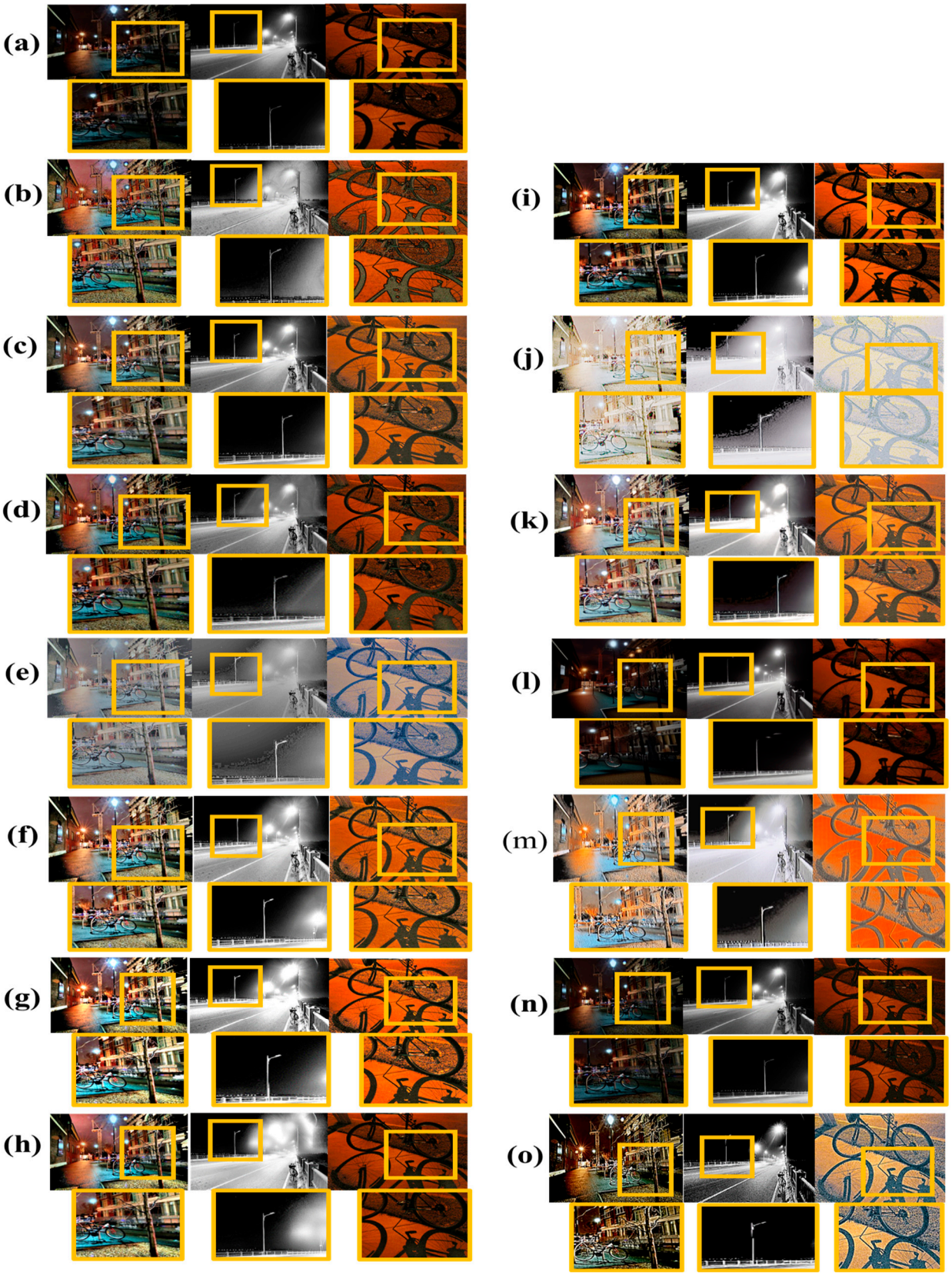


Figure 10. Comparison with state-of-the-art methods and the proposed method: (**a**) input; (**b**) Dong et al. [3]; (**c**) Ying et al. [41]; (**d**) Wang et al. [44]; (**e**) Jobson et al. [7]; (**f**) Ren et al. [42]; (**g**) Guo et al. [40]; (**h**) Li et al. [43]; (**i**) Huang et al. [1]; (**j**) Ma et al. [27]; (**k**) Wu et al. [36]; (**l**) Huang et al. [17]; (**m**) Jiang et al. [46]; (**n**) Lan et al. [25]; (**o**) proposed method.

3.2. Objective Assessment

While Figures 8–10 provide a subjective visual comparison between the state-of-the-art methods and the proposed approach, this section conducts a quantitative performance evaluation using two standard metrics: NIQE (Natural Image Quality Evaluator) [50] and UIQM (Underwater Image Quality Measure) [51], as well as BRISQUE (Blind/Referenceless Image Spatial Quality Evaluator) [52]. The NIQE metric assesses image quality by measuring statistical regularities, sharpness, and naturalness, where a lower score indicates higher image quality. Furthermore, BRISQUE (Blind/Referenceless Image Spatial Quality Evaluator) [52] evaluates image quality using pre-trained regression models based on natural scene statistics, where a lower score indicates superior enhancement performance. Conversely, UIQM [51] evaluates image quality based on contrast, colorfulness, and sharpness, where a higher score reflects superior recovery. Moreover, because low-images typically suffer from low contrast and color distortion, this paper used the UIQM [51] metric to thoroughly evaluate the enhancement performance. Although UIQM (Underwater Image Quality Measure) [51] was originally developed for underwater image enhancement, it is adopted in this work because low-light images share similar degradation characteristics with underwater scenes, such as severe illumination attenuation, low contrast, and color distortion. Specifically, UIQM evaluates an image across three complementary aspects—color balance, sharpness (edge content), and contrast—making it highly suitable for comprehensively assessing the visual quality and structural fidelity of enhanced low-light images. Tables 3–5 summarize the quantitative performance of the comparative methods and the proposed approach. Notably, certain metrics occasionally assign high scores to visually degraded outputs. For instance, although the enhanced images by Huang et al. [1] exhibit lower visual fidelity than those of Guo et al. [40], they occasionally yield better metric scores. Similarly, Ying et al. [41] achieve higher scores than Huang et al. [1], and Dong et al. [3] outperform Ren et al. [42] despite introducing visible artifacts. Furthermore, Li et al. [43] score higher than Jobson et al. [7], while Wang et al. [44] surpass Ying et al. [41]. The scores of Ma et al. [27] generally exceed those of Wu et al. [36]. Ren et al. [42] achieve superior performance compared to Jiang et al. [46], Huang et al. [17], and Lan et al. [25]. Overall, the proposed method achieves superior scores compared to existing techniques. As indicated by these quantitative metrics—though metric scores should be interpreted as relative references rather than absolute measures of visual quality—the proposed method demonstrates robust performance. Tables 3–5 present the average metric scores across the entire dataset [49]. As shown in Tables 3–5, the proposed method consistently yields superior average scores, further confirming its effectiveness and superiority in low-light image enhancement.

Table 3. Comparison of methods with the NIQE [50] metric according to dataset [49].

	Bicycle	Boat	Bottle	Bus	Car	Cat	Chair	Cup	Dog	Motorbike	People	Table
Huang et al. [1] NIQE [50]	18.609	18.689	19.92	19.171	19.64	19.415	19.617	20.232	19.401	19.154	19.451	19.661
Ying et al. [41] NIQE [50]	18.606	18.668	19.622	19.096	19.413	19.288	19.448	19.878	19.268	19.092	19.263	19.418
Dong et al. [3] NIQE [50]	17.365	17.565	18.46	17.574	18.259	18.533	18.173	18.853	18.24	17.656	18.138	18.101
Ren et al. [42] NIQE [50]	18.025	18.175	19.341	18.57	19.137	19.202	19.104	19.725	18.956	18.552	18.984	19.089
Guo et al. [40] NIQE [50]	17.567	17.803	18.937	18.19	18.654	18.763	18.656	19.418	18.504	18.145	18.514	18.752
Li et al. [43] NIQE [50]	18.49	18.62	19.524	19.072	19.232	19.009	19.127	19.755	18.868	19.103	19.083	19.276
Jobson et al. [7]												

Table 3. *Cont.*

	Bicycle	Boat	Bottle	Bus	Car	Cat	Chair	Cup	Dog	Motorbike	People	Table
NIQE [50] Wang et al. [44]	17.537	17.698	18.523	17.897	18.123	18.091	18.44	19.006	17.972	17.945	18.152	18.492
NIQE [50] Wu et al. [36]	18.211	18.403	19.093	18.549	18.819	18.777	18.853	19.438	18.642	18.655	18.665	18.916
NIQE [50] Ma et al. [27]	18.443	18.351	19.360	18.742	19.062	21.090	19.804	19.804	19.075	18.792	19.117	19.231
NIQE [50] Huang et al. [17]	17.667	17.885	19.106	18.197	18.935	18.961	18.900	19.604	18.805	18.231	18.747	18.887
NIQE [50] Jiang et al. [46]	19.422	19.024	19.934	19.497	19.656	19.688	19.817	20.233	19.603	19.614	19.728	19.810
NIQE [50] Lan et al. [25]	18.864	18.849	19.479	19.094	19.227	19.277	19.364	17.742	19.254	19.107	19.213	19.380
NIQE [50] PM	19.032	18.722	19.770	19.404	19.565	19.418	19.602	19.884	19.390	19.469	19.426	19.587
NIQE [50]	15.966	16.212	17.647	16.901	17.824	17.266	17.246	18.722	17.076	16.736	17.430	17.191

Table 4. Comparison of methods with the UIQM [51] metric according to dataset [49].

	Bicycle	Boat	Bottle	Bus	Car	Cat	Chair	Cup	Dog	Motorbike	People	Table
Huang et al. [1] UIQM [51]	1.649	1.503	1.617	1.656	1.612	1.57	1.559	1.521	1.562	1.644	1.627	1.571
Ying et al. [41] UIQM [51]	1.436	1.287	1.401	1.447	1.38	1.337	1.342	1.306	1.342	1.426	1.378	1.342
Dong et al. [3] UIQM [51]	1.604	1.483	1.575	1.621	1.571	1.528	1.529	1.491	1.529	1.602	1.569	1.541
Ren et al. [42] UIQM [51]	1.543	1.389	1.528	1.552	1.511	1.464	1.461	1.429	1.46	1.537	1.508	1.463
Guo et al. [40] UIQM [51]	1.587	1.445	1.56	1.603	1.549	1.5	1.506	1.47	1.499	1.586	1.548	1.517
Li et al. [43] UIQM [51]	1.525	1.388	1.478	1.52	1.465	1.437	1.432	1.378	1.429	1.511	1.474	1.441
Jobson et al. [7] UIQM [51]	1.475	1.407	1.354	1.451	1.427	1.411	1.338	1.263	1.426	1.438	1.42	1.353
Wang et al. [44] UIQM [51]	1.52	1.379	1.487	1.528	1.474	1.459	1.433	1.395	1.453	1.518	1.482	1.44
Wu et al. [36] UIQM [51]	1.415	1.268	1.365	1.386	1.311	1.287	1.310	1.270	1.308	1.403	1.327	1.304
Ma et al. [27] UIQM [51]	1.568	1.418	1.554	1.58	1.538	1.49	1.493	1.453	1.488	1.565	1.567	1.497
Huang et al. [17] UIQM [51]	1.674	1.525	1.650	1.685	1.662	1.552	1.543	1.501	1.528	1.621	1.595	1.542
Jiang et al. [46] UIQM [51]	1.330	1.203	1.268	1.320	1.229	1.190	1.221	1.187	1.205	1.313	1.269	1.230
Lan et al. [25] UIQM [51]	1.670	1.533	1.653	1.690	1.647	1.561	1.577	1.543	1.565	1.659	1.640	1.582
PM UIQM [51]	1.677	1.714	1.693	1.720	1.708	1.590	1.667	1.713	1.608	1.682	1.650	1.705

Table 5. Comparison of methods with the BRISQUE [52] metric according to dataset [49].

	Bicycle	Boat	Bottle	Bus	Car	Cat	Chair	Cup	Dog	Motorbike	People	Table
Huang et al. [1] BRISQUE [52]	23.356	21.987	22.294	22.989	22.086	22.886	22.286	21.471	22.822	23.033	22.492	22.280
Ying et al. [41] BRISQUE [52]	24.114	22.645	23.428	23.926	23.121	23.268	23.171	22.476	23.316	23.806	23.508	23.154
Dong et al. [3] BRISQUE [52]	26.315	24.616	25.370	25.293	25.263	25.650	25.289	24.385	25.717	25.917	26.671	25.402
Ren et al. [42] BRISQUE [52]	24.814	23.212	23.808	24.653	23.608	23.883	23.650	22.856	23.970	24.453	24.008	23.720
Guo et al. [40] BRISQUE [52]	25.342	23.681	24.600	25.1698	24.446	24.944	24.480	23.562	24.907	24.964	24.815	24.468
Li et al. [43] BRISQUE [52]	24.412	22.982	23.601	24.047	23.551	24.082	23.764	22.874	24.096	23.877	23.875	23.673

Table 5. *Cont.*

	Bicycle	Boat	Bottle	Bus	Car	Cat	Chair	Cup	Dog	Motorbike	People	Table
Jobson et al. [7]												
BRISQUE [52]	26.067	24.586	25.373	26.071	25.747	26.226	25.124	24.336	26.117	25.668	25.866	25.114
Wang et al. [44]												
BRISQUE [52]	25.107	23.510	24.532	25.051	24.451	25.209	24.425	23.405	25.033	24.729	24.962	24.321
Wu et al. [36]												
BRISQUE [52]	24.252	22.629	23.110	23.896	22.863	23.153	22.985	22.096	23.332	23.882	23.261	22.951
Ma et al. [27]												
BRISQUE [52]	25.217	23.509	25.072	25.425	24.843	24.628	24.541	24.095	24.548	25.608	25.057	24.503
Huang et al. [17]												
BRISQUE [52]	21.625	20.703	20.490	21.247	20.317	20.322	21.090	20.532	21.175	21.889	21.111	21.063
Jiang et al. [46]												
BRISQUE [52]	23.320	22.288	22.330	22.955	22.125	22.189	22.253	21.705	22.333	23.015	22.451	22.340
Lan et al. [25]												
BRISQUE [52]	22.688	21.612	21.369	22.273	21.059	21.218	21.368	20.740	21.523	22.275	21.429	21.375
PM												
BRISQUE [51]	19.024	18.651	21.370	19.688	20.865	19.697	22.504	21.642	22.852	22.892	22.399	22.339

Furthermore, Table 6 presents the overall average scores across the three evaluation metrics. As can be seen from Table 6, the proposed method demonstrates superior performance compared to other conventional methods.

Table 6. Comparison of methods with the average NIQE [50], UIQM [51], and BRISQUE [52] metrics according to dataset [49].

Metric (AVG)	Huang et al. [1]	Ying et al. [41]	Dong et al. [3]	Ren et al. [42]	Guo et al. [40]	Li et al. [43]	Jobson et al. [7]	Wang et al. [44]	Wu et al. [36]	Ma et al. [27]	Huang et al. [17]	Jiang et al. [46]	Lan et al. [25]	PM
NIQE [50]	19.413	19.255	18.076	18.905	18.492	19.097	18.156	18.7518	19.239	18.660	19.673	19.071	19.439	17.185
UIQM [51]	1.591	1.3687	1.554	1.487	1.531	1.457	1.397	1.464	1.330	1.518	1.570	1.247	1.610	1.677
BRISQUE [52]	22.499	23.328	25.491	23.886	24.615	23.736	25.525	24.561	23.201	24.754	20.964	22.442	21.577	21.160

4. Ablation Study

To validate the individual contributions of each core component in the proposed framework—specifically, the eigenvalue ratio-based gamma correction, the Laplacian transmission estimation, and the subsequent refinement step—this paper conducts a comprehensive ablation study. This paper evaluates several variants of our method by sequentially removing or replacing each component:

1. Eigenvalue-Based Gamma Correction: The eigenvalue-based adaptive gamma correction is omitted, and a fixed standard gamma value is applied. As a result, the model fails to dynamically adapt to the intrinsic dark characteristics of severely degraded inputs, leading to under-exposure or washed-out regions. This confirms the necessity of eigenvalue analysis for optimal global exposure adjustment.
2. Laplacian Feature-Based Transmission Map: Building upon the characteristic that the Laplacian operator is not invariant to local illumination, the proposed method estimates the transmission map through a combination of normalization and morphological erosion. This effectively compensates for the transmission estimation errors caused by local lighting variations in conventional Dark Channel Prior (DCP) [48] methods, thereby demonstrating that the proposed Laplacian-based transmission estimation makes a substantial contribution to the overall image enhancement.

Table 7 presents a quantitative evaluation of the performance at each stage using objective metrics on 100 test images. As demonstrated in Table 7, these results confirm the scientific validity of each proposed component.

Table 7. Stage-wise performance comparison using metrics NIQE [50], UIQM [51], and BRISQUE [52].

	Direct Gamma Correction		Proposed Method	
Color correction	NIQE [50]	18.913	NIQE [50]	18.237
	UIQM [51]	1.008	UIQM [51]	1.276
	BRISQUE [52]	22.249	BRISQUE [52]	23.237
Dehazing by DCP [48]	NIQE [50]	17.884	NIQE [50]	17.924
	UIQM [51]	1.341	UIQM [51]	1.501
	BRISQUE [52]	24.137	BRISQUE [52]	23.791
Dehazing by the proposed method	NIQE [50]	18.343	NIQE [50]	18.507
	UIQM [51]	1.247	UIQM [51]	1.545
	BRISQUE [52]	22.803	BRISQUE [52]	22.938
Jiang et al. [46]	NIQE [50]	18.740		
	UIQM [51]	1.375		
	BRISQUE [52]	23.708		

As quantitatively summarized in Tables 3–7, the full configuration, incorporating all three components, achieves good performance across all evaluation metrics (e.g., NIQE [50], UIQM [51], and BRISQUE [52]). This verifies that each module contributes complementarily and indispensably to the overall efficacy of the proposed pipeline.

5. Conclusions and Discussion

In this paper, a novel low-light image enhancement framework has been proposed to address issues arising from insufficient illumination. Specifically, the method combines eigenvalue-based adaptive gamma correction and a logarithmic function to effectively stretch image contrast. To mitigate the haze-like artifacts caused by the simultaneous amplification of noise during brightening, a dehazing-inspired denoising scheme is incorporated. By utilizing a Laplacian feature map for transmission map estimation—which does not capture edge components that are robust to illumination changes—the proposed framework successfully suppresses halo effects and color distortion. The primary contributions of this work are twofold: first, the integration of image eigenvalues enables natural contrast adjustment tailored to varying illumination conditions; second, the Laplacian feature map-based transmission map facilitates adaptive image refinement free from severe artifacts. Future work will focus on further refining adaptive contrast stretching and dehazing mechanisms to handle even more challenging low-light scenarios.

Funding: This research received no external funding.

Data Availability Statement: The data presented in this study are available on request from the corresponding author.

Conflicts of Interest: The author declares no conflicts of interest.

References

1. Huang, S.-C.; Cheng, F.-C.; Chiu, Y.-S. Efficient contrast enhancement using adaptive gamma correction with weighting distribution. *IEEE Trans. Image Process.* **2012**, *22*, 1032–1041. [CrossRef]
2. Ma, S.; Ma, H.; Xu, Y.; Li, S.; Lv, C.; Zhu, M. A low-light sensor image enhancement algorithm based on HSI color model. *Sensors* **2018**, *18*, 3583. [CrossRef]
3. Dong, X.; Pang, Y.; Wen, J. Fast efficient algorithm for enhancement of low lighting video. In Proceedings of the ACM SIGGRApH 2010 Posters, Los Angeles, CA, USA, 26–30 July 2010; pp. 1–6.

4. Tang, S.; Dong, M.; Ma, J.; Zhou, Z.; Li, C. Color image enhancement based on retinex theory with guided filter. In *Proceedings of the 2017 29th Chinese Control and Decision Conference (CCDC)*; IEEE: Piscataway, NJ, USA, 2017.
5. Fu, X.; Liao, Y.; Zeng, D.; Huang, Y.; Zhang, X.-P.; Ding, X. A probabilistic method for image enhancement with simultaneous illumination and reflectance estimation. *IEEE Trans. Image Process.* **2015**, *24*, 4965–4977. [CrossRef]
6. Yang, W.; Wang, S.; Fang, Y.; Wang, Y.; Liu, J. From fidelity to perceptual quality: A semi-supervised approach for low-light image enhancement. In *Proceedings of the IEEE/CVF Conference on Computer Vision and Pattern Recognition*; IEEE: Piscataway, NJ, USA, 2020.
7. Jobson, D.J.; Rahman, Z.-U.; Woodell, G.A. A multiscale retinex for bridging the gap between color images and the human observation of scenes. *IEEE Trans. Image Process.* **1997**, *6*, 965–976. [CrossRef]
8. Kimmel, R.; Elad, M.; Shaked, D.; Keshet, R.; Sobel, I. A variational framework for retinex. *Int. J. Comput. Vis.* **2003**, *52*, 7–23. [CrossRef]
9. Zhou, H.; Dong, W.; Liu, X.; Zhang, Y.; Zhai, G.; Chen, J. Low-light image enhancement via generative perceptual priors. In Proceedings of the AAAI Conference on Artificial Intelligence, Philadelphia, PA, USA, 25 February–4 March 2025; Volume 39.
10. Liu, X.; Xie, Q.; Zhao, Q.; Wang, H.; Meng, D. Low-light image enhancement by retinex-based algorithm unrolling and adjustment. *IEEE Trans. Neural Netw. Learn. Syst.* **2023**, *35*, 15758–15771. [CrossRef]
11. Wei, Z.; Wang, Y.; Sun, L.; Vasilakos, A.V.; Wang, L. ClassLIE: Structure-and illumination-adaptive classification for low-light image enhancement. *IEEE Trans. Artif. Intell.* **2024**, *5*, 4765–4775. [CrossRef]
12. Jiang, H.; Luo, A.; Liu, X.; Han, S.; Liu, S. Lightendiffusion: Unsupervised low-light image enhancement with latent-retinex diffusion models. In Proceedings of the European Conference on Computer Vision, Milan, Italy, 29 September–4 October 2024.
13. Yin, X.; Yu, Z.; Jiang, L.; Gao, X.; Sun, X.; Liu, Z.; Yang, X. Structure-guided diffusion transformer for low-light image enhancement. In Proceedings of the IEEE Transactions on Multimedia, Nantes, France, 30 June–4 July 2025.
14. Li, H.; Zhou, F.; Sun, X.; Hua, Y.; Han, J.; Zhang, L.-J. SAIGFormer: A Spatially-Adaptive Illumination-Guided Network for Low-Light Image Enhancement. *arXiv* **2025**, arXiv:2507.15520.
15. Zeng, J.; Yang, Q. PGRF: Physics-Guided Rectified Flow for Low-Light RAW Image Enhancement. *J. Imaging* **2025**, *11*, 393. [CrossRef]
16. Han, H.; Guo, T.; Zhang, L.; Su, Y.; Xu, Q.; Ye, Z. Towards Controllable Low-Light Image Enhancement: A Continuous Multi-Illumination Dataset and Efficient State Space Framework. *arXiv* **2026**, arXiv:2603.25296.
17. Huang, Y.; Liao, X.; Liang, J.; Quan, Y.; Shi, B.; Xu, Y. Zero-shot low-light image enhancement via latent diffusion models. In Proceedings of the AAAI Conference on Artificial Intelligence, Philadelphia, PA, USA, 25 February–4 March 2025; Volume 39.
18. Chen, T.; Liu, D. Low light image enhancement based on Retinex theory and diffusion model. In Proceedings of the 2024 8th International Conference on Digital Signal Processing, Hangzhou, China, 23–25 February 2024.
19. Wu, Y.; Wang, G.; Wang, Z.; Yang, Y.; Li, T.; Zhang, M.; Li, C.; Shen, H.T. JoReS-Diff: Joint retinex and semantic priors in diffusion model for low-light image enhancement. In Proceedings of the 32nd ACM International Conference on Multimedia, Melbourne, Australia, 28 October–1 November 2024.
20. Zou, W.; Gao, H.; Yang, W.; Liu, T. Wave-mamba: Wavelet state space model for ultra-high-definition low-light image enhancement. In Proceedings of the 32nd ACM International Conference on Multimedia, Melbourne, Australia, 28 October–1 November 2024.
21. Wu, X.; Lai, Z.; Zhou, J.; Hou, X.; Pedrycz, W.; Shen, L. Light-aware contrastive learning for low-light image enhancement. *ACM Trans. Multimed. Comput. Commun. Appl.* **2024**, *20*, 1–24. [CrossRef]
22. Li, W.; Wu, X.; Guan, Y.; Lin, S.; Ding, N.; Wang, Q.; Tang, Y. GLMA: Global-to-Local Mamba Architecture for Low-Light Image Enhancement. *Appl. Sci.* **2025**, *15*, 10931. [CrossRef]
23. Cai, Y.; Bian, H.; Lin, J.; Wang, H.; Timofte, R.; Zhang, Y. Retinexformer: One-stage retinex-based transformer for low-light image enhancement. In Proceedings of the IEEE/CVF International Conference on Computer Vision, Paris, France, 1–6 October 2023.
24. Yin, M.; Yang, J. ILR-Net: Low-light image enhancement network based on the combination of iterative learning mechanism and Retinex theory. *PLoS ONE* **2025**, *20*, e0314541. [CrossRef]
25. Lan, G.; Ma, Q.; Yang, Y.; Wang, Z.; Wang, D.; Li, X.; Zhao, B. Efficient diffusion as low light enhancer. In Proceedings of the Computer Vision and Pattern Recognition Conference, Nashville, TN, USA, 11–15 June 2025.
26. Zeng, X.; Zhu, L.; Yang, W.; Leung, H.; Wang, S.; Kwong, S. Low-Light Image Enhancement via Diffusion Models with Semantic Priors of Any Region. In *Proceedings of the IEEE Transactions on Circuits and Systems for Video Technology*; IEEE: Piscataway, NJ, USA, 2025.
27. Ma, L.; Ma, T.; Liu, R.; Fan, X.; Luo, Z. Toward fast, flexible, and robust low-light image enhancement. In *Proceedings of the IEEE/CVF Conference on Computer Vision and Pattern Recognition*; IEEE: Piscataway, NJ, USA, 2022.
28. Hou, J.; Zhu, Z.; Hou, J.; Liu, H.; Zeng, H.; Yuan, H. Global structure-aware diffusion process for low-light image enhancement. *Adv. Neural Inf. Process. Syst.* **2023**, *36*, 79734–79747. [CrossRef]
29. Weng, J.; Yan, Z.; Tai, Y.; Qian, J.; Yang, J.; Li, J. Mamballie: Implicit retinex-aware low light enhancement with global-then-local state space. *Adv. Neural Inf. Process. Syst.* **2024**, *37*, 27440–27462. [CrossRef]
30. Ding, B.; Sun, B.; Sun, X. Low-Light Remote Sensing Image Enhancement via Priors Guided End-to-End Latent Residual Diffusion. *Remote Sens.* **2025**, *17*, 3193. [CrossRef]

31. He, M.; Wang, R.; Zhang, M.; Lv, F.; Wang, Y.; Zhou, F.; Bian, X. SwinLightGAN a study of low-light image enhancement algorithms using depth residuals and transformer techniques. *Sci. Rep.* **2025**, *15*, 12151. [CrossRef]
32. Sun, L.; Bao, Y.; Zhai, J.; Liang, J.; Zhang, Y.; Wang, K.; Paudel, D.P.; Van Gool, L. Low-light image enhancement using event-based illumination estimation. In *Proceedings of the IEEE/CVF International Conference on Computer Vision*; IEEE: Piscataway, NJ, USA, 2025.
33. Wu, Y.; Wang, G.; Liu, S.; Yang, Y.; Li, W.; Tang, X.; Gu, S.; Li, C.; Shen, H.T. Towards a flexible semantic guided model for single image enhancement and restoration. *IEEE Trans. Pattern Anal. Mach. Intell.* **2024**, *46*, 9921–9939. [CrossRef]
34. Wang, S.; Zeng, S.; Gu, T.; Zhang, Z.; Zhang, R.; Ding, S.; Zhang, J.; Wang, J.; Tan, X.; Xie, Y.; et al. From Enhancement to Understanding: Build a Generalized Bridge for Low-light Vision via Semantically Consistent Unsupervised Fine-tuning. In *Proceedings of the IEEE/CVF International Conference on Computer Vision*; IEEE: Piscataway, NJ, USA, 2025.
35. Wang, Y.; Liu, Z.; Liu, J.; Xu, S.; Liu, S. Low-light image enhancement with illumination-aware gamma correction and complete image modelling network. In *Proceedings of the IEEE/CVF International Conference on Computer Vision*; IEEE: Piscataway, NJ, USA, 2023.
36. Wu, W.; Weng, J.; Zhang, P.; Wang, X.; Yang, W.; Jiang, J. Uretinex-net: Retinex-based deep unfolding network for low-light image enhancement. In *Proceedings of the IEEE/CVF Conference on Computer Vision and Pattern Recognition*; IEEE: Piscataway, NJ, USA, 2022.
37. Xu, X.; Wang, R.; Fu, C.W.; Jia, J. Snr-aware low-light image enhancement. In *Proceedings of the IEEE/CVF Conference on Computer Vision and Pattern Recognition*; IEEE: Piscataway, NJ, USA, 2022.
38. Yan, Q.; Feng, Y.; Zhang, C.; Pang, G.; Shi, K.; Wu, P.; Dong, W.; Sun, J.; Zhang, Y. HVI: A new color space for low-light image enhancement. In Proceedings of the Computer Vision and Pattern Recognition Conference, Nashville, TN, USA, 11–15 June 2025.
39. Yi, X.; Xu, H.; Zhang, H.; Tang, L.; Ma, J. Diff-retinex: Rethinking low-light image enhancement with a generative diffusion model. In *Proceedings of the IEEE/CVF International Conference on Computer Vision*; IEEE: Piscataway, NJ, USA, 2023.
40. Guo, X. LIME: A method for low-light image enhancement. In Proceedings of the 24th ACM International Conference on Multimedia, Amsterdam, The Netherlands, 15–19 October 2016.
41. Ying, Z.; Li, G.; Gao, W. A bio-inspired multi-exposure fusion framework for low-light image enhancement. *arXiv* **2017**, arXiv:1711.00591.
42. Ren, Y.; Ying, Z.; Li, T.H.; Li, G. LECARM: Low-light image enhancement using the camera response model. *IEEE Trans. Circuits Syst. Video Technol.* **2018**, *29*, 968–981. [CrossRef]
43. Li, C.; Guo, J.; Porikli, F.; Pang, Y. LightenNet: A convolutional neural network for weakly illuminated image enhancement. *Pattern Recognit. Lett.* **2018**, *104*, 15–22. [CrossRef]
44. Wang, S.; Zheng, J.; Hu, H.-M.; Li, B. Naturalness preserved enhancement algorithm for non-uniform illumination images. *IEEE Trans. Image Process.* **2013**, *22*, 3538–3548. [CrossRef]
45. Ma, L.; Ma, T.; Xu, C.; Liu, J.; Fan, X.; Luo, Z.; Liu, R. Learning with self-calibrator for fast and robust low-light image enhancement. In *Proceedings of the IEEE Transactions on Pattern Analysis and Machine Intelligence*; IEEE: Piscataway, NJ, USA, 2025.
46. Jiang, B.; Wang, X.; Yang, N.; Liu, Y.; Chen, X.; Wu, Q. Semantic-aware low-light image enhancement by learning from multiple color spaces. *Appl. Sci.* **2025**, *15*, 5556. [CrossRef]
47. Lee, H. Sandstorm image enhancement using image-adaptive eigenvalue and brightness-adaptive dark channel network. *Symmetry* **2022**, *14*, 2310. [CrossRef]
48. He, K.; Sun, J.; Tang, X. Single image haze removal using dark channel prior. *IEEE Trans. Pattern Anal. Mach. Intell.* **2010**, *33*, 2341–2353. [CrossRef]
49. Loh, Y.P.; Chan, C.S. Getting to know low-light images with the exclusively dark dataset. *Comput. Vis. Image Underst.* **2019**, *178*, 30–42. [CrossRef]
50. Mittal, A.; Soundararajan, R.; Bovik, A.C. Making a "completely blind" image quality analyzer. *IEEE Signal Process. Lett.* **2012**, *20*, 209–212. [CrossRef]
51. Panetta, K.; Gao, C.; Agaian, S. Human-visual-system-inspired underwater image quality measures. *IEEE J. Ocean. Eng.* **2015**, *41*, 541–551. [CrossRef]
52. Mittal, A.; Moorthy, A.K.; Bovik, A.C. No-reference image quality assessment in the spatial domain. *IEEE Trans. Image Process.* **2012**, *21*, 4695–4708. [CrossRef]

Disclaimer/Publisher's Note: The statements, opinions and data contained in all publications are solely those of the individual author(s) and contributor(s) and not of MDPI and/or the editor(s). MDPI and/or the editor(s) disclaim responsibility for any injury to people or property resulting from any ideas, methods, instructions or products referred to in the content.